Available online at www.sciencedirect.com
ScienceDirect
Surface & Coatings Technology 202 (2008) 3913–3920
SURFACE & COATINGS TECHNOLOGY
www.elsevier.com/locate/surfcoat

The preparation of calcium phosphate coatings on titanium and nickel–titanium by rf-magnetron-sputtered deposition: Composition, structure and micromechanical properties

V.F. Pichugin [a,*], R.A. Surmenev [a], E.V. Shesterikov [a], M.A. Ryabtseva [a], E.V. Eshenko [a], S.I. Tverdokhlebov [a], O. Prymak [b], M. Epple [b]

[a] *Theoretical and Experimental Physics Department, Tomsk Polytechnic University, 634050 Tomsk, Russia*
[b] *Inorganic Chemistry and Center for Nanointegration Duisburg-Essen (CeNIDE), University of Duisburg-Essen, D-45117 Essen, Germany*

Received 21 October 2007; accepted in revised form 31 January 2008
Available online 16 February 2008

Abstract

Thin calcium phosphate coatings with a thickness of 0.09 to 2.7 μm were prepared by radio-frequency magnetron sputtering deposition on NiTi and Ti substrates at a substrate temperature of 500 °C in argon atmosphere. Scanning electron microscopy (SEM) showed that the surface structure is uniform and dense without visible defects (pores and microcracks). Rutherford backscattering spectroscopy (RBS) and energy-dispersive X-ray spectroscopy (EDX) confirmed that the coating contains calcium, phosphorus, and oxygen with a uniform composition. Crystallographically, the coating consists of crystalline hydroxyapatite which is also supported by infrared spectroscopy. The mechanical characteristics of the coating were measured by nanoindentation (Vickers indenter), giving a nanohardness of 10 GPa and a Young's modulus of 110 GPa. The strength of adhesion of the calcium phosphate coating to the metallic substrates depended on the coating's thickness and decreased for a thickness larger than 1.6 μm. No difference was observed between NiTi and Ti substrates.

Keywords: Calcium phosphate coating; rf-magnetron sputtering; Adhesion strength

1. Introduction

Hydroxyapatite, $Ca_{10}(PO_4)_6(OH)_2$, is an important geological calcium phosphate mineral and also constitutes the inorganic component (biomineral) of human hard tissue, i.e. of teeth and bone [1,2]. Due to its excellent biocompatibility, it is well established as coating for metallic implants in medicine, e.g. for hip endoprostheses and for tooth implants.

Many methods are known to produce such biocompatible coatings on metals for biomedical applications: High-temperature plasma-spraying [3–12], dip-coating/crystallization techniques [13–16], electrophoretic deposition [17–20], laser deposition [21], and micro-arc techniques. However, each method has its own limitations, often caused by low adhesion strength to the substrate and also by difficulties to control the phase composition of the coating during the deposition.

Radio-frequency magnetron sputtering (rf-magnetron sputtering) to deposit calcium phosphate coatings on metals was introduced at the end of the 20th century [22–31]. It was reported that bone marrow cells reproduced faster on such a calcium phosphate coating than on an uncovered implant surface [22,23]. The response of different bone-specific cell lines to such sputter-coated surfaces was also favorable, e.g. for osteoblast-like cells [32], osteoblast precursor cells [33] and rat bone marrow cells [34]. These investigations also showed that the calcium phosphate coating had a high adhesion strength to the metallic substrate. The chemical composition of the coating was very similar to that of the initial target used for sputtering, including a multicomponent target. Consequently, there are many possibilities to control the composition of the coating by changing the sputter target material and by variation of the sputtering conditions (e.g. the discharge power, the working gas, and the substrate temperature).

* Corresponding author. Tel.: +7 3822 563 819.
E-mail address: pichugin@tpu.ru (V.F. Pichugin).

0257-8972/$ - see front matter © 2008 Elsevier B.V. All rights reserved.
doi:10.1016/j.surfcoat.2008.01.038

Besides its ability to induce bone-bonding to an implant [35,36], an important function of a biocompatible coating is the protection of the human organism against harmful metal ions which may be released from the metallic substrate. Therefore, such a coating should be dense and pore-free with a high strength of adhesion to the metallic substrate. These concerns are of special importance when an implant alloy contains heavy metals like nickel or chromium [37,38]. Ideally, these elements must not be released into the surrounding tissue but be restrained by the coating. rf-magnetron sputtering is a very promising technique in this respect because it allows to prepare thin, dense and pore-free coatings. The state of the art has recently been reviewed by Yang et al. [39] and Xu et al. [28]. Notably, if both titanium and calcium phosphate targets are used, even graded coatings can be accomplished [40]. The frequently applied orthopaedic titanium alloy Ti6Al4V was coated with hydroxyapatite by Long et al. [41] and Xu et al. [28].

Here we present a thorough investigation on the microstructure, the chemical and crystallographic composition and the micromechanical properties of calcium phosphate coatings deposited by rf-magnetron sputtering on nickel–titanium (NiTi) [42] and titanium (Ti) as typical implant materials.

2. Materials and methods

Plates ($10\cdot10\cdot0.5$ mm^3) of NiTi (superelastic, "medical grade" from Memory Metalle GmbH, Germany, with $A_P = 21.5$ °C [preceded by an endothermal peak at 0.2 °C] and $M_p = 16.4$ °C) and Ti (technically pure, 99.58 wt.% Ti, 0.1 wt.% O, 0.15 wt.% Fe, 0.05 wt.% C, 0.04 wt.% N, 0.08 wt.% Si; from Goodfellow) were used as substrates. Before sputtering, all samples were mechanically polished to the roughness class 10 ($R_a < 0.1$ μm).

An installation type Cathode 1M where the rf-magnetron sputtering device was situated in a vacuum chamber was used to prepare the calcium phosphate coating. The following parameters were applied in the sputtering process: Operation frequency of the rf-generator 13.56 MHz, working gas argon (0.5 Pa), incident power of the rf-generator 2 kW, reflected power 200 W, and distance between substrate and magnetron target 50 mm. The sputtering chamber was evacuated to less than $5\cdot10^{-5}$ Pa and then argon was introduced as a sputter gas. By variation of the sputtering time from 10 to 320 min, the coating thickness was increased from 0.09 to 2.7 μm, respectively. In exploratory experiments, these parameters were found to be optimal for deposition of the calcium phosphate coating. We used a target of microcrystalline synthetic hydroxyapatite prepared from a powder with a particle size of 80 nm by pressing at 70 MPa and subsequent sintering at 1000 °C in air for 1 h. The metallic substrate was heated to 500 °C by the rf-plasma in all experiments, and its temperature was controlled with a Pt/PtRh thermocouple. This set of parameters with a high value of the rf-power was fixed in the experiments because we aimed at a hydroxyapatite coating with high crystallinity [43].

For scanning electron microscopy, we used a scanning electron microscope type ESEM Quanta 400 FEG from FEI, equipped with energy-dispersive X-ray analysis (EDX; EDS analysis system Genesis 4000, S-UTW-Si(Li) detector), operating in high vacuum. A sputtering of the samples with gold was not necessary due to the small thickness of the coating that resulted in a sufficient electrical conductivity to avoid electrostatic charging.

The coating thickness was determined with a mechanical profilometer Talysurf 5 (Tyler-Hobson, England). The coating thickness was determined by shielding a part of the sample from the sputtering target, thereby preventing the coating formation on this part of the sample. The thickness of the coating was determined by measuring the profile of the resulting edge and determination of the step height. The profilometer vertical resolution was 10 nm and the horizontal resolution was 2 μm (determined by the radius of scanning needle).

For Rutherford backscattering spectrometry (RBS) of α-particles, all samples were arranged on a calibrated ruler in the vacuum chamber with the parameters $E(^4\mathrm{He}) = 1.7$ MeV, scattering angle 175°, and spectrometer energy resolution 11 keV. The diameter of the analyzing ^{4}He beam was approximately 2 mm, i.e. it covered a representative area of the sample. The elemental concentration profiles in the coating were computed from the RBS data with a custom-made program. In order to improve the experimental accuracy, we used the yield of scattering ions from each substrate as internal standard. X-ray powder diffraction (XRD) was carried out with a Siemens D500 diffractometer operating with Cu K_α radiation ($\lambda = 1.5406$ Å) at 40 kV and 20 mA in Bragg–Brentano mode. As references we used the following entries from the ICDD database: Synthetic hydroxyapatite (#9-0432) and titanium (#44-1294). For infrared spectroscopy we used a Bruker Vertex 70 FTIR instrument in the range of 400–4000 cm^{-1} (resolution 4 cm^{-1}; averaging of 20 scans).

The mechanical parameters of the coating were determined by dynamic nanoindentation with a Vickers Nano Hardness tester (CSEM Instruments). The immersion speed of the Vickers diamond pyramid with an angle between opposite faces of 136° was 5 mN min^{-1} and the time of a loading–unloading cycle was 2 min. Eight indentations were made on the coating surface of each sample and then an average value was calculated for each sample. The adhesion parameters were determined with a Micro Scratch Tester (CSEM Instruments) equipped with a Rockwell indenter with a tip radius of 20 μm. The adhesion strength was measured in three ways: 1) acoustic emission data, 2) control of the friction coefficient, and 3) visual inspection of the damaged area after the experiment with an optical microscope. The scratching parameters were chosen as follows: Indenter lateral motion speed 7 mm min^{-1}, loading rate 2 N min^{-1}, maximum applied load 2 N.

3. Results and discussion

Calcium phosphate coatings were deposited on titanium and on superelastic nickel–titanium. Unless explicitly stated, all following results were identical for both substrates. The thickness of the coating was determined by mechanical profilometry. A coating growth rate of 0.5 μm h^{-1} was derived from these measurements. This compares well to Ref. [44]

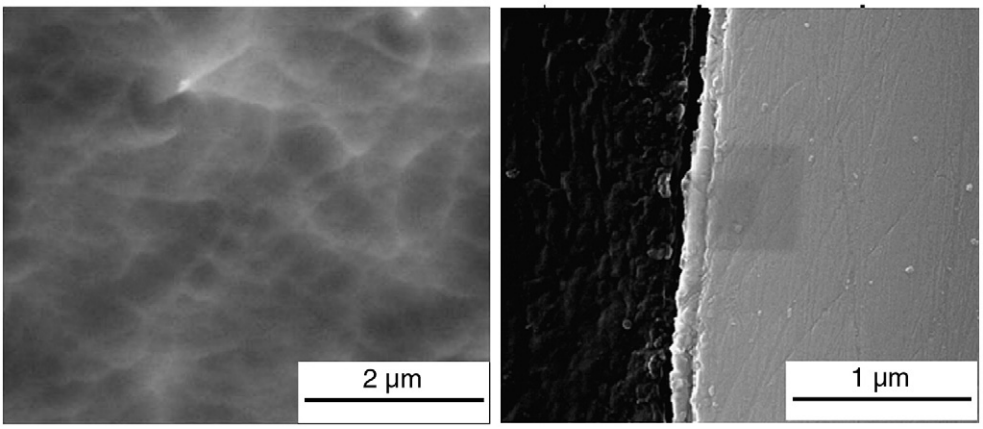

Fig. 1. Scanning electron micrograph of calcium phosphate coatings. Left: Frontal view of a coating on a NiTi substrate. Right: Cross sectional view of a 100 nm thick coating (center) on a titanium substrate (right), deposited at 30 W for 2 h. The coating is dense and pore-free in both viewing directions.

where the rate of the calcium phosphate coating growth depended on the rf-power and was approximately 0.3–1.5 μm h^{-1} at 200–400 W in an argon atmosphere, and also to Ref. [45] where growth rates of 0.29–1.75 μm h^{-1} were found at rf-powers of 200–800 W.

Scanning electron microscopy showed that the calcium phosphate coating was dense and practically free of pores (Fig. 1).

The elemental distribution over the coating was determined by Rutherford backscattering spectrometry (RBS). Fig. 2 shows a typical partial spectrum of α-particles backscattered from a calcium phosphate coating on titanium, showing only calcium, phosphorus and oxygen. Note that hydrogen cannot be detected by this method due to its low atomic weight. In Fig. 3, the computed elemental concentration profile is shown as a function of the coating thickness. The average content of the elements in the coating was 49±1 at.% oxygen, 34±2 at.% calcium, and 17±2 at.% phosphorus. These values were almost constant within the coating and did not depend on the metallic substrate (Ti or NiTi).

A molar Ca:P ratio of about 1.8:1 was derived from the values shown in Fig. 3. The Ca:P ratio was also determined by EDX analysis to 1.77:1, i.e. close to the value obtained using RBS technique. The stoichiometric Ca:P ratio in pure hydroxyapatite is 1.67:1 [2,46]. The deviation from the stoichiometric ratio in hydroxyapatite can be explained by the rf-magnetron sputtering mechanism in accordance with Refs. [43,47]. The higher Ca:P-ratio may be due to 1) calcium implantation into the growing coating, 2) phosphorus escaping from the chamber as P_2O_5 before the deposition, or 3) preferable re-sputtering of phosphorus on the way through the plasma sheath to the substrate or re-sputtering phosphorus away from the growing coating by heavier impinging particles [43]. In other studies, where the authors used a semi-qualitative EDX analysis to determine the Ca:P ratio in magnetron sputter-deposited coatings, they found values of 1.7 to 2 [43,48,49]. According to Han et al. [50], the ratio of atoms incorporated from a multi-component target is strongly influenced by the argon pressure during sputtering. At higher pressure, the ions with lower atomic mass are scattered to a larger extent by the argon ions than ions with higher atomic mass [51].

In Fig. 4, an X-ray diffraction pattern of an as-deposited coating with a thickness of 1.5 μm is shown. Besides peaks from the titanium substrate, only slightly broadened

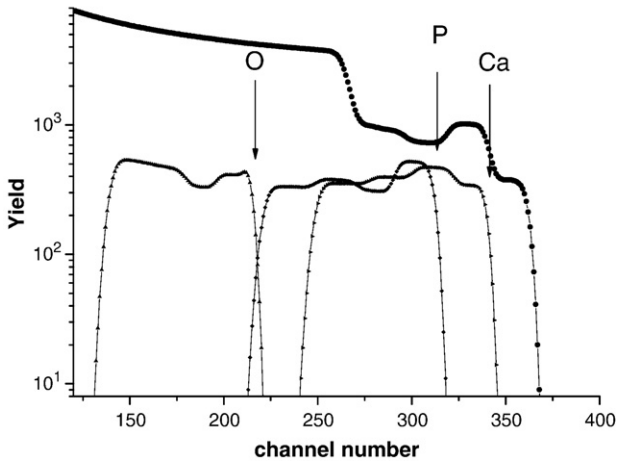

Fig. 2. A RBS partial spectrum of a calcium phosphate coating on titanium with a thickness of 1.1 μm. The coating consists of calcium, phosphorus and oxygen.

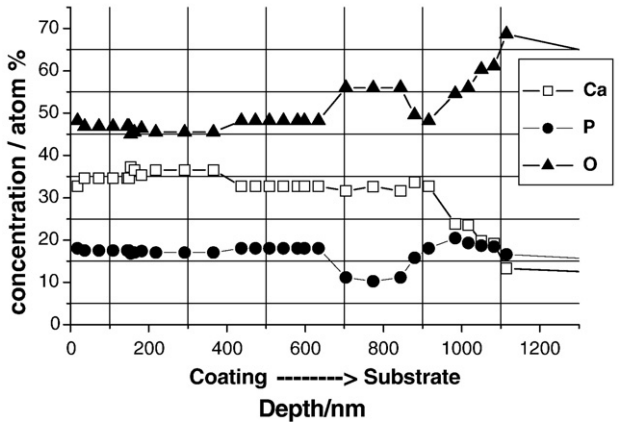

Fig. 3. The elemental composition of the calcium phosphate coating (thickness: 1.1 μm) on a titanium substrate as a function of depth computed from Rutherford backscattering spectrometry data.

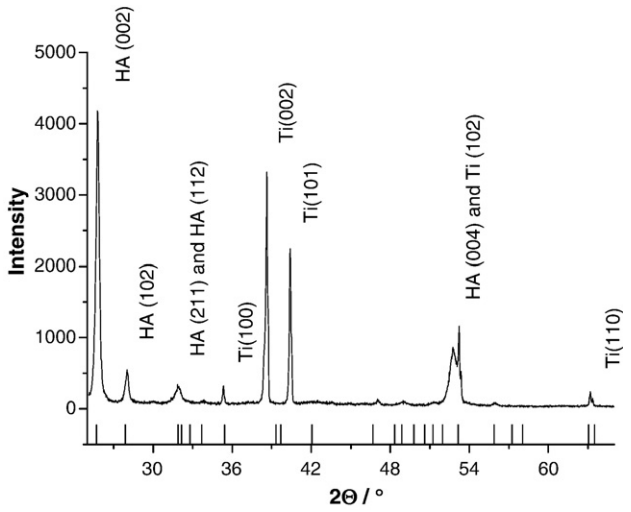

Fig. 4. An X-ray powder diffractogram of a calcium phosphate coating on titanium (thickness: 1.5 μm). Besides the substrate (Ti), only hydroxyapatite (HA) was found. The theoretical peak positions of hydroxyapatite are indicated at the bottom of the spectrum.

hydroxyapatite peaks, indicating a good crystallinity, were found. We note that the high intensity of the (002) peak at 25.78°2Θ indicates a preferred orientation of hydroxyapatite in this direction. No other high-temperature phases like β-tricalcium phosphate (β-TCP; $Ca_3(PO_4)_2$), tetracalcium phosphate (TTCP; $Ca4(PO_4)_2O$) or calcium oxide (CaO) which can occur in the plasma-spray process [10,12] were found. Note that amorphous calcium oxide [52] may be formed by such sputtering processes as reported in Ref. [31]. This may explain the fact that the observed Ca:P ratios are higher than that of stoichiometric hydroxyapatite.

Other authors also reported a coating growth with a (001) preferential orientation for hydroxyapatite coatings obtained by magnetron sputtering [26,28,45,47,48,53,54]. One of the main factors that influences the nature of a growing coating is the substrate temperature during deposition. Nelea et al. found that a substrate temperature of 550 °C gave a crystalline calcium phosphate [43]. Ozeki et al. suggested that the preferential growth of hydroxyapatite in the (001) direction is due to the fact that the *c-axis* (0.6884 nm) in hydroxyapatite is shorter than the *a-axis* (0.9418 nm) [54]. Onuma et al. ascribed the preferential HA growth in the (001) direction with a cluster growth model, where $Ca_9(PO_4)_6$ clusters are situated along the *c-axis* [53].

Infrared spectroscopy of the coating was possible by sputtering it on elemental silicon which is almost transparent for infrared radiation. Thereby, the coating could be observed without the need to detach it from the substrate. The IR spectra of the as-deposited coatings were corrected by subtraction of the IR spectrum obtained for an uncoated silicon substrate. The IR spectrum of the coating showed bands assigned to phosphate and in general strongly resembles the IR spectrum of hydroxyapatite (Fig. 5) [55]. The absence of the O–H band (expected around 3500 cm^{-1}) may be due to the deposition process. As reported by Yang et al. [56], the thermal dehydroxylation of hydroxyapatite occurs at about 800 °C, and hydroxyapatite converts to oxyhydroxapatite, with the formula $Ca_{10}(PO_4)_6(OH)_{2-2x}O_xV_x$, where V is a vacancy and $x<1$ [57,58]. This may well occur under the conditions of the sputtering process. It was also reported that the hydroxyapatite structure can be restored by annealing of the as-deposited coating in different atmospheres, e.g. in air or water vapor [33].

All coatings for a potential medical application require a sufficient mechanical strength, i.e. adhesion strength and cohesive resistance. In particular, the mechanical properties are very important with respect to the long-term stability of an implant.

Therefore, we determined Young's modulus (E), nanohardness (H) and contact stiffness (S) of as-deposited coatings using nanoindentation, i.e. the penetration of a diamond indenter into the coating with continuously increasing load was measured.

The nanohardness H was determined by Eq. (1):

$$H = \frac{P_{\max}}{A_c} \tag{1}$$

with $P_{\max}$ the maximum indentation force and A_c the indented area after unloading. The contact stiffness S of each coating was determined from the unloading curve according to Eq. (2):

$$S = \frac{dP}{dh} \tag{2}$$

where dP is the load alteration and dh is the corresponding depth alteration.

The Young's modulus E was determined in the same way like S, i.e. on the unloading curve according to Eq. (3) [59]

$$E = \sqrt{\frac{\pi}{2}}\frac{S}{\sqrt{A_c}} \tag{3}$$

where S is the contact stiffness of the investigated material.

Nanohardness H and Young's modulus E as a function of the coating thickness are shown in Fig. 6. The obtained data

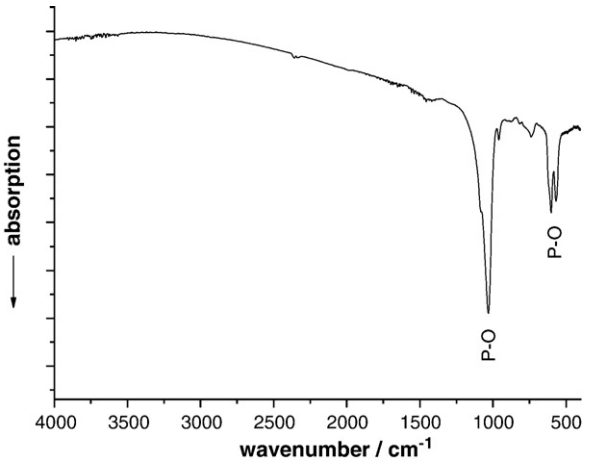

Fig. 5. Infrared spectrum of a calcium phosphate coating on silicon. All bands could be assigned to the PO_4^{3-} group (v_3, 1032 cm^{-1}; v_4, 607 cm^{-1}; v_4, 564 cm^{-1}). The weak band around 1500 cm^{-1} indicates minor amounts of incorporated carbonate from the atmosphere. The weak band at 750 cm^{-1} belongs to silicon.

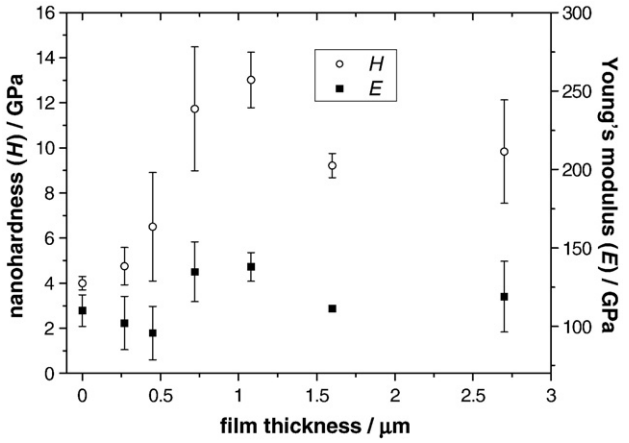

Fig. 6. Nanohardness (H) and Young's modulus (E) of calcium phosphate coatings on titanium as a function of the coating thickness. The values given for a coating thickness of zero correspond to pure titanium.

indicate that the titanium substrate influences the nanohardness of the calcium phosphate coating only if its thickness is smaller than 700 nm. The nanohardness of a titanium substrate is about 4 GPa [60] and its Young's modulus is 110 GPa [61], in good agreement with our values (Table 1). The nanohardness of Ti is considerably smaller than that of the thin calcium phosphate coating whereas Young's modulus is comparable (nanohardness about 10 GPa and Young's modulus about 110 GPa). The computed values of H, E, and S are summarized in Table 1. For a NiTi substrate, very similar results were obtained with the exception that NiTi had a higher nanohardness (12.0±0.7 GPa) than titanium but a comparable Young's modulus (90±4 GPa). This value depends on the phase composition of the NiTi but is in good accordance with the literature (70 GPa) [62,63]. We ascribe the scatter in the experimental results to the sensitivity of the nanohardness technique, i.e. the results obtained depend on the substrate surface roughness, the indenter state and other parameters. Although all substrates were carefully polished before sputtering, we assume that there are variations in the substrate surface morphology which caused the observed scatter.

Our results (Fig. 6) indicate that the effect of substrate material vanishes when the coating thickness becomes larger than about 700 nm. This is in accordance with Refs. [28,41,45] where calcium phosphate was deposited on Ti6Al4V. In Ref. [28], the coatings were deposited at the substrate temperature of 550 °C which is close to that used in our study. The coating failure analysis revealed that the calcium phosphate coating had an excellent adhesive strength to the Ti6Al4V substrate. To investigate the coating failure, a load in the range from 0.3 to 15 N at 3 N min^{-1} over a length of 10 mm was applied [28]. Although we applied other parameters to investigate the coating performance (a loading rate of 2 N min^{-1} and a scratch distance of 7 mm), we could confirm the excellent adhesion of the sputter-deposited calcium phosphate coating if its thickness does not exceed 1.6 µm (see below).

Load–displacement curves obtained for the titanium substrate and for the calcium phosphate coating on titanium are shown in Fig. 7. The load–displacement curves showed that the deformation behavior of the coating as well as that of the titanium substrate was plastic with some elastic components, i.e. when the load was removed, a part of the deformation relaxed. Nanohardness and contact stiffness of the calcium phosphate coatings were larger than those of the titanium substrate (Table 1). The substrate influenced H, E and S only if the coating thickness was smaller than 0.7 µm. We conclude that the nanohardness and the Young's modulus of the pure calcium phosphate coating itself are about 10 GPa and 110 GPa, respectively. We also found that the value of the nanohardness decreased when the indenter penetration depth increased, a phenomenon known as Indentation Size Effect [64,65].

There are only a few reports on the application of nanohardness measurements to rf-magnetron-deposited calcium phosphate coatings. Furthermore, it is very difficult to compare these results,

Table 1
Nanohardness H, Young's modulus E and contact stiffness S of calcium phosphate coatings on titanium prepared by rf-magnet ron sputtering

Coating thickness / µm	Penetration depth / µm	Ratio of penetration depth to coating thickness	H / GPa	E / GPa	S / mN nm^{-1}
0.09	0.055±0.015	0.610	11±4	100±20	0.0342±0.0004
0.27	0.165±0.010	0.609	5±1	100±10	0.121±0.004
0.45	0.202±0.010	0.450	7±2	100±20	0.098±0.002
0.72	0.150±0.010	0.210	11.8±2.0	130±20	0.099±0.003
1.08	0.152±0.020	0.140	13.0±1.2	140±10	0.096±0.005
1.60	0.130±0.030	0.080	9.2±0.5	111±1	0.094±0.002
2.70	0.162±0.010	0.060	9±2	120±20	0.103±0.005
Non-coated titanium substrate	0.236±0.020	–	4.0±0.3	110±10	0.140±0.010
Non-coated NiTi substrate	0.170±0.005	–	12.0±0.7	90±4	0.065±0.001

The results are given as average±standard deviation.

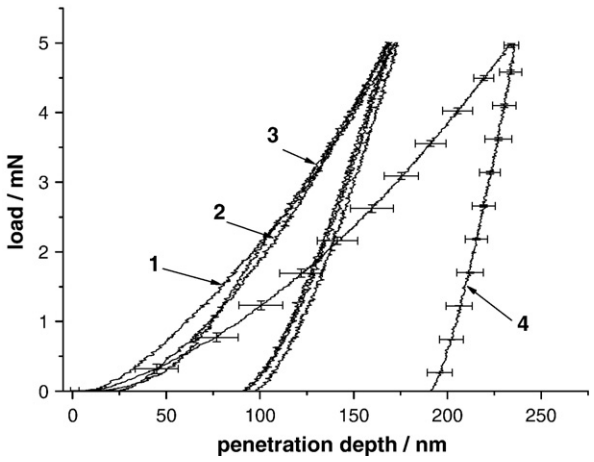

Fig. 7. Load–displacement curves from nanoindentation obtained for a calcium phosphate coating of 1.6 µm thickness on titanium (curves 1, 2, and 3) and a non-coated titanium substrate (curve 4).

because the coating procedures were different and, on the other hand, the authors used different techniques and experimental equipment to determine the mechanical properties. For instance, Nelea et al. [26] reported a nanohardness of 3.4–4 GPa and a Young's modulus of 122–150 GPa. Although they used another substrate, i.e. TiAlFe, and a Berkovich indenter tip, their values are in good agreement with our values. Nelea et al. compared the mechanical properties of magnetron sputter-deposited and laser-deposited coatings. The magnetron-deposited coatings had higher values of nanohardness and Young's modulus than laser-deposited coatings [43].

The adhesion strength between the calcium phosphate coating and the substrate was determined by the scratch test method. This also allowed us to estimate the cohesive resistance. Calcium phosphate coatings deposited on Ti and NiTi substrates were studied.

The coating did not show signs of disruption in the vicinity of the scratch, and the coating did not exfoliate even at a maximal load of 2 N (Fig. 8). When the indenter penetrated into the substrate, no signs of bursting of the coating along a scratching direction were found. A similar behavior was observed when other samples (with the same or a smaller thickness) were investigated; these coatings were only impressed into the coating–metal

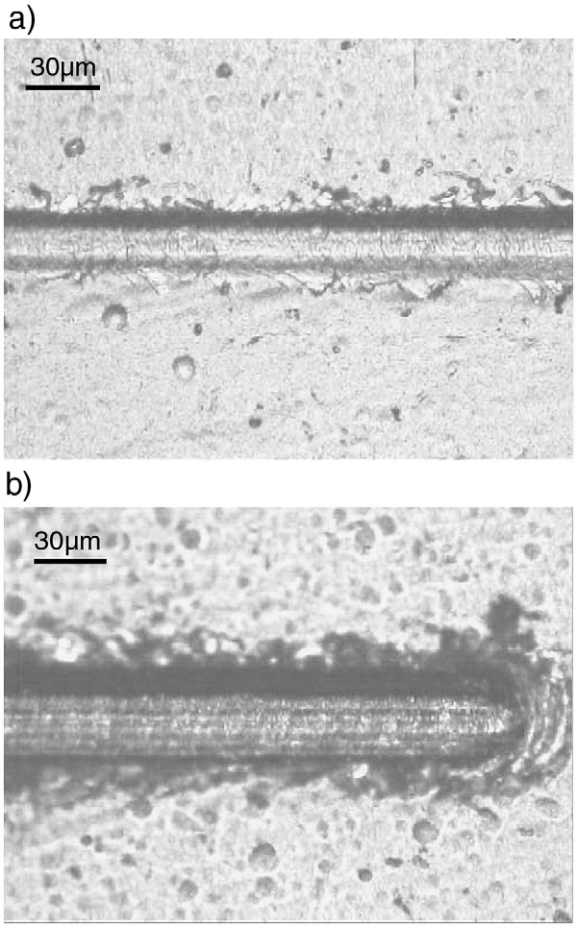

Fig. 8. Light-microscopic images of scratch tests on a calcium phosphate coating (thickness 1.6 μm) on titanium. The images a) and b) were taken at 0.87 N and 2 N, respectively. The coating was not damaged during the scratch test experiment but merely impressed into the substrate. There are tracks of a deformative wave ahead of the scratching direction. Equivalent results were obtained for calcium phosphate on NiTi.

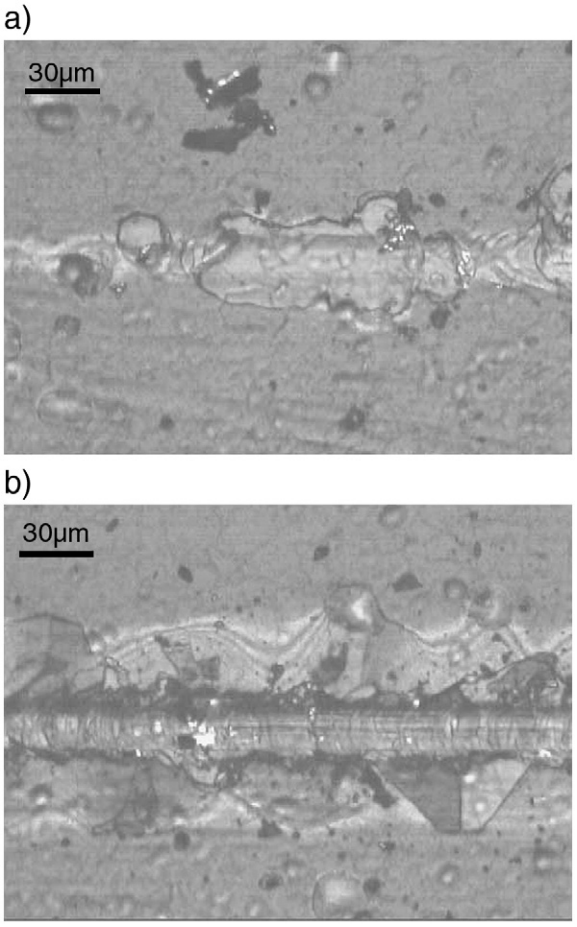

Fig. 9. Light-microscopic images of scratch tests on a calcium phosphate coating (thickness 2.7 μm) on titanium. The images a) and b) were taken at loads of 0.42 and 0.66 N, respectively. The coating was clearly damaged during the scratch test experiment. There are clear signs of exfoliation and bursting of the calcium phosphate coating.

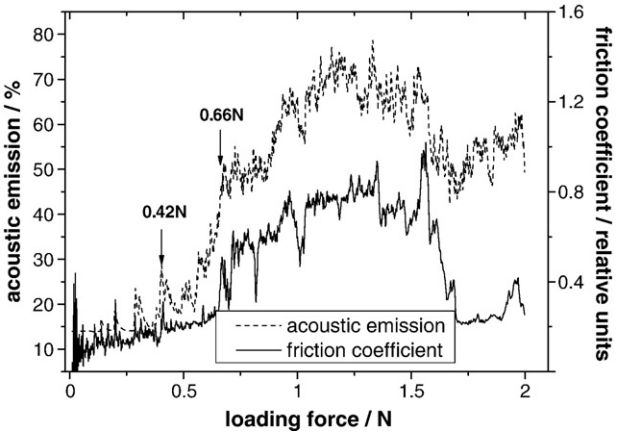

Fig. 10. A pattern of a dynamic scratch test on the surface of a calcium phosphate coating on a titanium substrate (thickness 2.7 μm).

interface and no signs of coating failure were seen at the edges of the scratch. We conclude that all coatings with a thickness of less than 1.6 μm possess both a sufficient adhesion strength and cohesive resistance.

The high values of adhesion strength can be explained by the fact that during calcium phosphate coating growth, the ions ejected from the target form a chemisorbed state with the surface atoms of the substrate. For Ti and NiTi substrates, the surfaces are always covered with a very thin oxide layer. This leads to a strong interaction (with a binding energy above 0.5 eV) between substrate and coating [66].

The mode of damaging of a calcium phosphate coating with a thickness greater than 1.6 μm differed from that of the thinner calcium phosphate coatings. The destruction of the coatings with a thickness of less than 1.6 μm occurred only after its perforation, whereas thicker coatings collapsed by exfoliation, splits and chips along the scratching direction (Fig. 9). With a thickness of 2.7 μm, cracking and detachment of the coating surface layers started at a loading force of 0.42 N. When the force reached 0.66 N, the coating burst, and at a force of 1 N, the calcium phosphate coating was completely damaged. The acoustic emission signal at a force of 0.42 N also indicated the detachment of the coating from the substrate (Fig. 10). This was observed for all forces up to 2 N.

Finally, we observed that upon bending the superelastic NiTi, the coating was not detached, i.e. it is well suited for this superelastic material. Chen et al. showed by investigation of the tensile adhesion strength that the adhesion strength of a graded Ti/hydroxyapatite coating was much better than that of monolithic hydroxyapatite [40]. Here we found using a qualitative scratch-test technique that the adhesion strength of a monolithic hydroxyapatite coating depends on the coating thickness. Although we cannot determine the absolute value of the strength of adhesion of the hydroxyapatite coating, we conclude that the adhesion strength of the coatings with a thickness up to 1.6 μm is larger than 40 MPa because no signs of a failure of the hydroxyapatite-coating were found even at a loading force of 2 N [40]. If the coating thickness is larger than 1.6 μm, the adhesion strength dramatically decreases, and the mode of coating failure also changes. If the coating becomes too thick, its internal cohesive strength is not sufficient to retain its integrity upon strong mechanical loading.

4. Conclusions

By rf-magnetron sputtering, it is possible to prepare thin, uniform and crystalline coatings of hydroxyapatite on titanium as a classical implant material and on nickel–titanium which also finds applications as superelastic or shape-memory implant material. The mechanical parameters of the coatings are best if they are thinner than 1.6 μm. On the other hand, the effect of the substrate is only important if the film is thinner than about 1 μm. We finally conclude that rf-magnetron sputtering is well suited to coat implant metals and alloys with a thin layer of bioactive calcium phosphate. Further investigations are needed to understand the biological performance of rf-magnetron-deposited coatings, including its ability to prevent the leaching of metal ions from the substrate and also its corrosion resistance in body fluids.

References

[1] S. Weiner, H.D. Wagner, Annu. Rev. Mater. Sci. 28 (1998) 271.
[2] S.V. Dorozhkin, M. Epple, Angew. Chem. Int. Ed. 41 (2002) 3130.
[3] E. Lugscheider, G. Berger, M. Knepper, R. Sicking, A. Nyland, Bioceramics 8 (1995) 317.
[4] J. Hemmerle, A. Oncag, S. Erturk, J. Biomed. Mater. Res. 36 (1997) 418.
[5] Y. Han, K. Xu, G. Montay, T. Fu, J. Lu, J. Biomed. Mater. Res. 60 (2002) 511.
[6] A.K. Lynn, D.L. DuQuesnay, Biomaterials 23 (2002) 1937.
[7] A.K. Lynn, D.L. DuQuesnay, Biomaterials 23 (2002) 1947.
[8] L. Sun, C.C. Berndt, K.A. Khor, H.N. Cheang, K.A. Gross, J. Biomed. Mater. Res. 62 (2002) 228.
[9] Y.Z. Yang, J.L. Ong, J. Biomed. Mater. Res. 64A (2003) 509.
[10] O. Prymak, D. Bogdanski, S.A. Esenwein, M. Köller, M. Epple, Mat.-wiss. u. Werkstofftech. 35 (2004) 346.
[11] M. Topic, T. Ntsoane, R.B. Heimann, Surface Coatings Technol. 201 (2006) 3633.
[12] R.B. Heimann, Surface Coatings Technol. 201 (2006) 2012.
[13] K.A. Gross, C.S. Chai, G.S.K. Kannangara, B. Ben-Nissan, J. Mater. Sci. Mater. Med. 9 (1998) 839.
[14] F. Barrère, P. Layrolle, C.A. van Blitterswijk, K. de Groot, Bone 25 (1999) 107S.
[15] P. Habibovic, F. Barrère, C.A. van Blitterswijk, K. de Groot, P. Layrolle, J. Am. Ceram. Soc. 85 (2002) 517.
[16] J. Choi, D. Bogdanski, M. Köller, S.A. Esenwein, D. Müller, G. Muhr, M. Epple, Biomaterials 24 (2003) 3689.
[17] M. Kumar, H. Dasarathy, C. Riley, J. Biomed. Mater. Res. 45 (1999) 302.
[18] H. Monma, O. Nemoto, S. Takahashi, H. Kobayashi, J. Electroceramics 4 (S1) (1999) 135.
[19] S. Rößler, A. Sewing, M. Stölzel, R. Born, D. Scharnweber, M. Dard, H. Worch, J. Biomed. Mater. Res. 64A (2003) 655.
[20] H. Urch, S. Franzka, D. Dahlhaus, N. Hartmann, E. Hasselbrink, M. Epple, J. Mater. Chem. 16 (2006) 1798.
[21] S. Griforescu, C. Ristoscu, G. Socol, E. Axente, F. Feugeas, I.N. Mihailescu, Rom. Rep. Physics 57 (2005) 1003.
[22] S. Vercaigne, J.G.C. Wolke, N. Jansen, Clinic. Oral. Imp. Res. 11 (2000) 305.
[23] S. Vercaigne, J.G.C. Wolke, N. Jansen, Clinic. Oral. Imp. Res. 11 (2000) 314.
[24] E.M. Burke, J.D. Haman, J.J. Weimer, A.B. Cheney, J.M. Rigsbee, L.C. Lucas, J. Biomed. Mater. Res. 57 (2001) 41.
[25] J.G.C. Wolke, J.P.C.M. van der Waerden, H.G. Schaeken, J.A. Jansen, Biomaterials 24 (2003) 2623.
[26] V. Nelea, C. Morosanu, M. Iliescu, I.N. Mihailescu, Surface Coatings Technol. 173 (2003) 315.
[27] B. Feddes, J.G.C. Wolke, A.M. Vredenberg, J.A. Jansen, Biomaterials 25 (2004) 633.
[28] S. Xu, J. Long, L. Sim, C.H. Diong, K. Ostrikov, Plasma Proc. Polym. 2 (2005) 373.
[29] K. Ostrikov, Rev. Modern Phys. 77 (2005) 489.
[30] Y.T. Zhao, Z. Zhang, Q.X. Dai, D.Y. Lin, S.M. Li, Surface Coatings Technol. 200 (2006) 5354.
[31] J. Long, L. Sim, S. Xu, K. Ostrikov, Chem. Vap. Deposition 13 (2007) 299.
[32] X. Lu, Y. Leng, J. Biomed. Mater. Res. 66A (2003) 677.
[33] Y. Yang, J.D. Bumgardner, R. Cavin, D.L. Carnes, J.L. Ong, J. Dent. Res. 82 (2003) 449.
[34] Y.G. Yan, J.G.C. Wolke, Y.B. Li, J. Jansen, Clin. Oral Implants Res. 18 (2007) 345.
[35] G. Daculsi, R.Z. LeGeros, M. Heughebaert, I. Barbieux, Calcif. Tissue Int. 46 (1990) 20.
[36] W. Cao, L.L. Hench, Ceramics Int. 22 (1996) 493.
[37] M. Uo, F. Watari, A. Yokoyama, H. Matsuno, T. Kawasaki, Biomaterials 20 (1999) 747.
[38] L. Budinger, M. Hertl, Allergy 55 (2000) 108.
[39] Y. Yang, K.H. Kim, J.L. Ong, Biomaterials 26 (2005) 327.

[40] M. Chen, D. Liu, C. You, X. Yang, Z. Cui, Surface Coatings Technol. 201 (2007) 5688.
[41] J.D. Long, S. Xu, J.W. Cai, N. Jiang, J.H. Lu, K.N. Ostrikov, C.H. Diong, Mat. Sci. Eng. C 20 (2002) 175.
[42] L. Yahia, Shape memory implants, Springer, Berlin, 2000.
[43] V. Nelea, C. Morosanu, M. Iliescu, I.N. Mihailescu, Appl. Surf. Sci. 228 (2004) 346.
[44] K. van Dijk, J. Verhoeven, C.H.M. Marée, F.H.P.M. Habraken, J.A. Jansen, Thin Solid Films 304 (1997) 191.
[45] K. van Dijk, H.G. Schaeken, J.G.C. Wolke, C.H.M. Maree, F.H.P.M. Habraken, J. Verhoeven, J.A. Jansen, J. Biomed. Mater. Res. 29 (1995) 269.
[46] J.C. Elliot, Structure and chemistry of the apatites and other calcium orthophosphates, vol. 18, Elsevier, Amsterdam, 1994.
[47] J.L. Ong, G.N. Raikar, T.M. Smoot, Biomaterials 18 (1997) 1271.
[48] J.G.C. Wolke, K. van Dijk, H.G. Schaeken, K. de Groot, J.A. Jansen, J. Biomed. Mater. Res. 28 (1994) 1477.
[49] Y. Yonggang, J.G.C. Wolke, L. Yubao, J.A. Jansen, J. Biomed. Mater. Res. A 76 (2006) 744.
[50] S.H. Han, H.J. Kim, I.K. Kang, J.J. Lee, J. Mater. Sci. 28 (1993) 3267.
[51] K. van Dijk, H.G. Schaeken, J.G.C. Wolke, J.A. Jansen, F.H.P.M. Habraken, J. Verhoeven, C.H.M. Marée, Surf. Coatings Technol. 76–77 (1995) 206.
[52] S. Sivaram, Chemical Vapor Deposition: Thermal and Plasma Deposition of Electronic Materials, Int. Thompson Publ. Inc., New York, 2000.
[53] K. Onuma, A. Ito, Chem. Mater. 10 (1998) 3346.
[54] K. Ozeki, T. Yuhta, H. Aoki, I. Nishimura, Y. Fukui, Biomed. Mater. Eng. 10 (2000).
[55] D. Tadic, M. Epple, Biomaterials 25 (2004) 987.
[56] Y. Yang, K.H. Kim, C.M. Agrawal, J.L. Ong, J. Dent. Res. 82 (2003) 833.
[57] E.E. Berry, C.B. Baddiel, Spectrochim. Acta A23 (1976) 1781.
[58] Y.C. Tsui, C. Doyle, T.W. Clyne, Biomaterials 19 (1998) 2015.
[59] W.S. Oliver, G.M. Pharr, J. Mater. Res. 7 (1992) 1564.
[60] G.B. de Souza, C.E. Foerster, S.L.R. da Silva, F.C. Serbena, C.M. Lepienski, C.A. dos Santos, Surf. Coatings Technol. 191 (2005) 76.
[61] W.D. Callister, Materials Science and Engineering, John Wiley and Sons, New York, 2000.
[62] G.Q. Song, Q.P. Sun, Smart Mater. Struct. 9 (2000) 693.
[63] I. Mihalcz, Periodica Polytechnica Ser. Mech. Eng. 45 (2001) 75.
[64] D. Tabor, The Hardness of Metals, Clarendon Press, Oxford, 1951.
[65] M. Atkinson, J. Mater. Sci. 30 (1995) 1728.
[66] A. von Keudell, J. Plasma Sources Sci. Technol. 9 (2000) 445.